Calibration of the Airborne Visible/Infrared Imaging Spectrometer in the Laboratory

Thomas G. Chrien, Robert O. Green, Christopher J. Chovit,
Michael L. Eastwood, and Charles M. Sarture

Jet Propulsion Laboratory, California Institute of Technology, Pasadena, CA 91109

1.0 Introduction

Imaging spectrometry data must be spectrally, radiometrically and geometrically calibrated in order to 1) derive physical parameters from measured spectral radiance, 2) compare data acquired from different regions and at different times, 3) compare and analyze the imaging spectrometry data with data acquired from other calibrated sensors, and 4) compare and analyze data with results from computer models. The calibration of AVIRIS data is the process by which laboratory characterization data are applied to raw instrument data (digitized number versus spectral channels) to produce quantitative spectra (radiance versus wavelength) for each image pixel in units of spectral radiance. The AVIRIS sensor and calibration process are described by Vane (Vane et al., 1993) and the application of the calibration data to the raw digital data is described by Green (Green et al., 1991). This calibration process is validated for in-flight performance of the sensor using a rigorous ground-truth campaign (Green et al. 1996).

This workshop paper reviews the laboratory characterization data set that is used in the AVIRIS calibration process. The laboratory measurements used to acquire the calibration data are divided into three classes: 1) spectral calibration, 2) radiometric calibration, and 3) spatial calibration.

2.0 Spectral Calibration

The collection of spectral calibration data for AVIRIS was first described by Vane (Vane et al., 1987) and then updated by Chrien (Chrien et al., 1990). The spectral calibration requirement for AVIRIS is 0.1 nm accuracy in channel center wavelength and channel full width at half maximum (FWHM) (Green, 1995a) based on a sensitivity to the ubiquitous narrow solar and atmospheric absorptions in the upwelling spectral radiance. The method is to measure the response of each of the 224 AVIRIS channels to narrow bandwidth light (~1 nm FWHM) as the light is scanned in wavelength across the spectral response of the channel. A monochromator and collimator, as shown in Figure 1a, are used to measure the spectral response. Figure 1b shows a typical example of the Gaussian function fit to a channel spectral response from which the center wavelength and FWHM channel width are derived. The wavelength calibration of the monochromator is traced to mercury vapor, neon and krypton emission lamps.

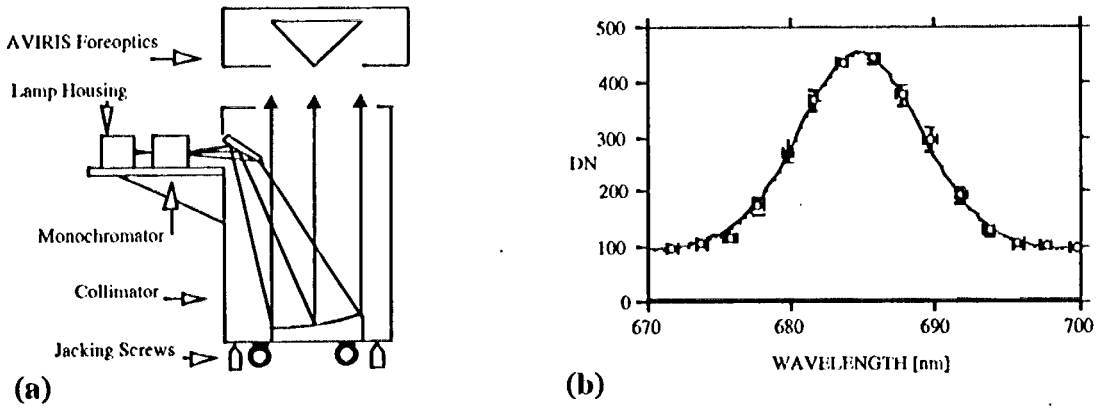

FIGURE 1. a) Laboratory spectral calibration setup. b) Typical spectral response function with error bars and best-fit Gaussian curve from which center wavelength, FWHM bandwidth, and uncertainties are derived.

The spectral response data are collected for each of the 224 spectral channels as the monochromator wavelength increments through the AVIRIS spectral range. The center wavelength and FWHM width for each channel are determined, with uncertainties, from a Gaussian fit to the raw response curve for that channel. The center wavelength for each of the 224 spectral channels' fit is shown in Figure 2 (bold line), where discontinuity in the line denotes the spectral overlap between the four AVIRIS spectrometers. The associated uncertainty in the determination of center wavelength is shown on the same plot by reading the right axis.

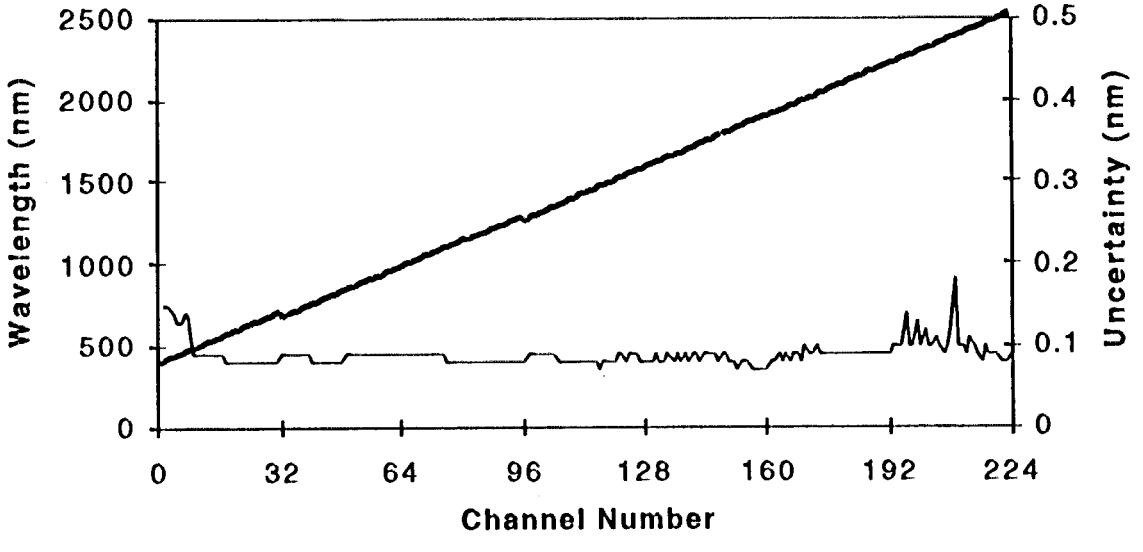

FIGURE 2. Derived center wavelengths for each AVIRIS channel (bold line), read from left axis, and associated uncertainty in center wavelength knowledge (normal line), read from right axis.

The best-fit Gaussian FWHM bandwidth for each of the 224 spectral channels is shown in Figure 3 (bold line). The associated uncertainty in the determination of FWHM bandwidth

is shown on the same plot by reading the right axis. A majority of the channels meet the calibration uncertainty goal of less than 0.1 nm in absolute knowledge of center wavelength and FWHM channel width.

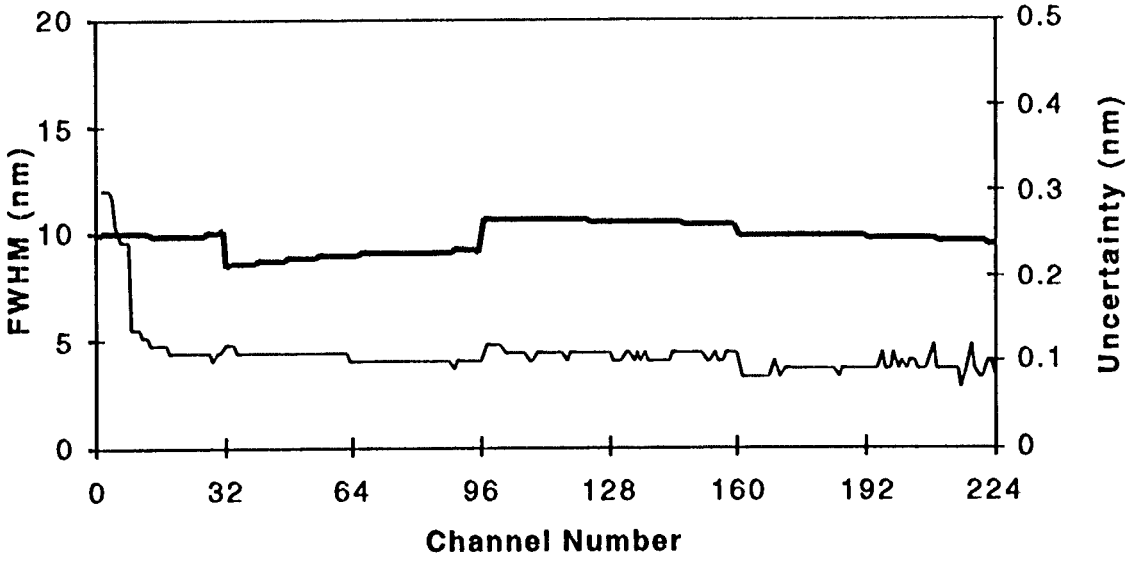

FIGURE 3. Derived FWHM bandwidth for each AVIRIS channel (bold line), read from left axis, and associated bandwidth uncertainty (normal line), read from right axis.

The in-flight calibration of the spectral response has been validated using a least-squares curve fit to atmospheric features over carefully characterized field targets such as Lunar Lake, Nevada, and Rogers Dry Lake, California (Green, 1995b; Green et al., 1993). The AVIRIS onboard calibration system can also be used to monitor minute changes in the spectral response by computing the transmittance of the spectrally feature-full filters and observing shifts with respect to filter data acquired at the time of the laboratory calibration (Chrien et al., 1995).

3.0 Radiometric Calibration

The absolute radiometric calibration of the AVIRIS sensor is determined by measuring the radiometric response of the sensor to a standard of known spectral radiance. The standard is constructed from an irradiance standard lamp and a reflectance standard panel as shown in Figure 4. The standards are purchased with calibrations traceable to the National Institute of Standards and Technology (NIST). The spectral radiance of the standard, $L(\lambda)$, is computed using EQ 1:

$$L(\lambda) = \frac{E(\lambda)R(\lambda)}{\pi} \qquad \text{(EQ 1)}$$

where $E(\lambda)$ is the lamp irradiance at a distance of 50 cm from a panel and $R(\lambda)$ is the Bidirectional reflectance factor (BRF) as measured in the 0°, 45° configuration. The spectral radiance of the standard is shown in Figure 5 along with the associated percent uncertainty

as computed using the error propagation in Equation 1. The AVIRIS sensor views the standard directly. The AVIRIS response is computed as the mean of 1000 digital number (dn) samples per spectral channel. The standard deviation of the 1000 samples divided by the mean is the percent uncertainty in the response. The mean and percent uncertainty in the response are shown in Figure 6.

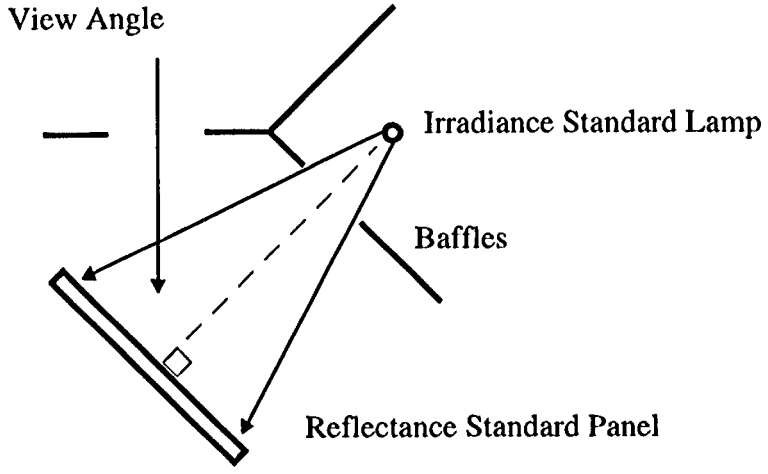

FIGURE 4. Viewing geometry for NIST-traceable radiance standard.

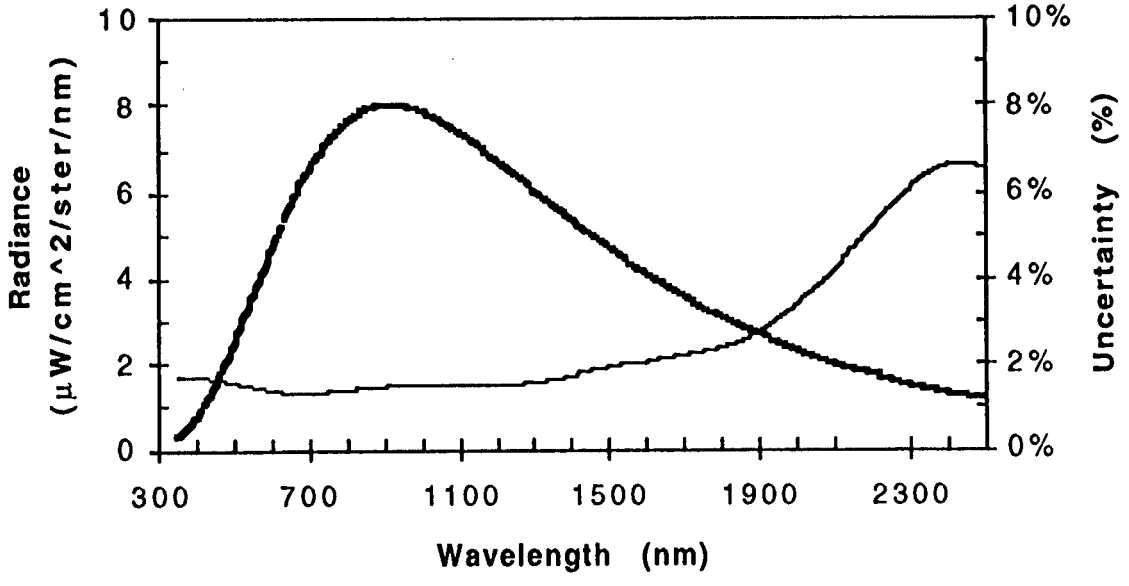

FIGURE 5. NIST traceable radiance standard target radiance (bold line), read from left axis, and percent radiometric uncertainty (normal line), read from right axis.

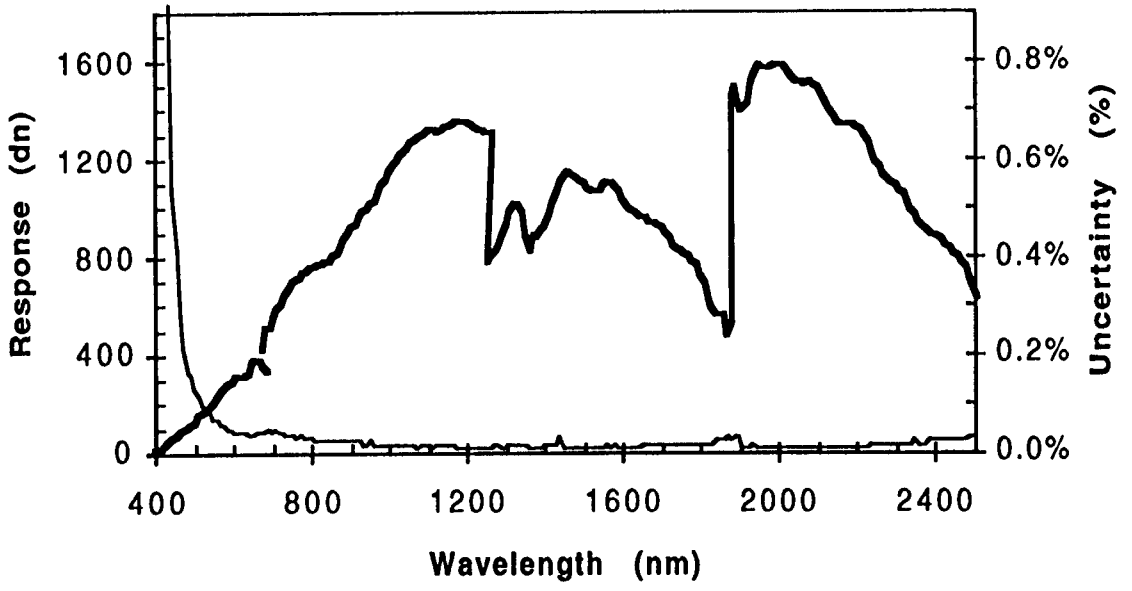

FIGURE 6. AVIRIS digital number (dn) response to NIST-traceable radiance standard (bold line), read from left axis, and percent uncertainty of response due to measurement noise (normal line), read from right axis.

Radiometric calibration coefficients are computed by dividing the standard radiance by the sensor dn response. The results are shown in Figure 7 along with the root-sum-square (RSS) uncertainty of standard radiance and sensor response.

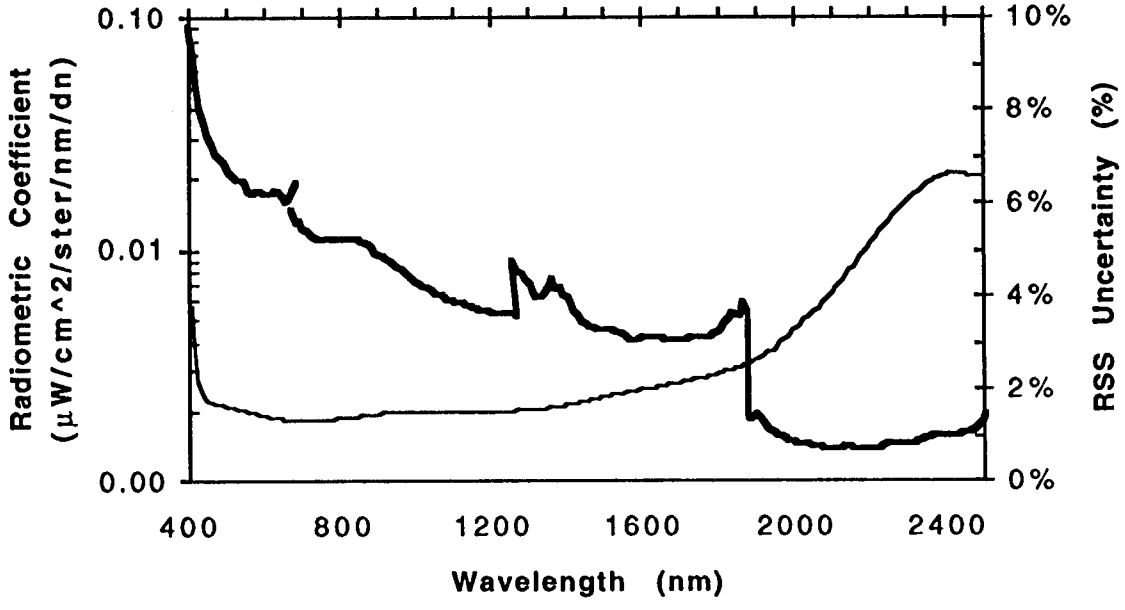

FIGURE 7. Radiometric calibration coefficients derived by dividing the NIST-traceable standard radiance by the AVIRIS radiometric response to the same standard (bold line), read from left axis, and root sum square (RSS) percent uncertainty (normal line), read from right axis.

The RSS uncertainty is dominated by the radiance standard uncertainty, except at wavelengths below 430 nm where the sensor response uncertainty becomes significant. These radiometric gain coefficients are applied to inflight image data to produce calibrated image radiance. An additional onboard calibrator correction factor may be applied to compensate for minor drifts in spectrometer response (Green, 1993).

The radiometric gain coefficients are validated in-flight using a series of calibration experiments scheduled for the start, middle, and end of the flight season (Green et al., 1996; Green et al., 1993). The field experiment predicts the upwelling radiance at the AVIRIS sensor via an independent calibration path that relies on measurements of playa reflectance, atmospheric optical depth, and the MODTRAN3 radiative transfer code (Anderson et al., 1995). Figure 8 shows the percent difference (dotted line) between the inflight calibration experiment predicted radiance and the AVIRIS measured, laboratory calibrated radiance. The percent uncertainty of the measurement (bold line) derived as the RSS of calibration uncertainty (normal line) and the inverse of the signal-to-noise ratio of the playa target spectra are shown for comparison. This indicates that the radiometric calibration uncertainty is approximately the right magnitude. The actual difference from the prediction is influenced by factors including errors in the MODTRAN3 line list and algorithm, errors in the AVIRIS spectral calibration, and instabilities in the field spectrometer used in the playa reflectance measurements. The point to note is that in spite of the many unknowns in the comparison, the level of agreement is better than the error analysis derived uncertainty in many parts of the spectrum. This suggests that the NIST calibration uncertainty may be overstated, especially in the 2100 to 2450 nm spectral region.

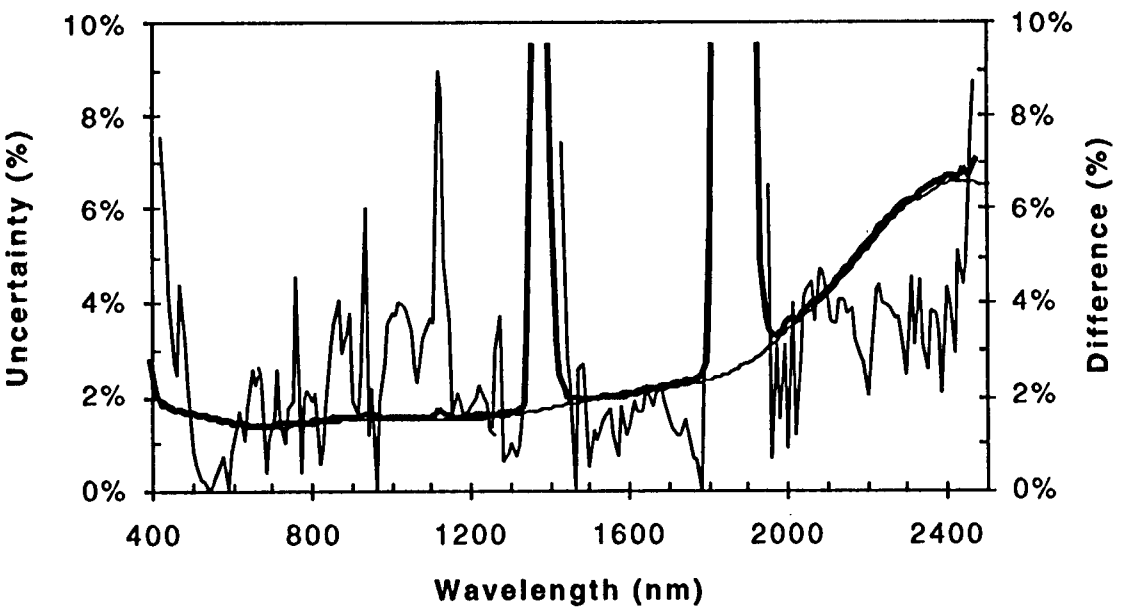

FIGURE 8. Measurement uncertainty (bold line), read from left axis, derived as the RSS of calibration uncertainty (normal line), read from right axis, and the percent variation in the measured spectrum due to instrument noise, atmospheric, and playa variability compared to the percentage difference between the laboratory calibrated spectra and the MODTRAN3 constrained independent prediction of radiance.

4.0 Spatial Calibration

The spatial calibration of AVIRIS describes the spatial sampling and geometric response function (GRF) of the sensor (Chrien and Green, 1993). Response data are collected while translating an illuminated narrow slit across the instantaneous field-of-view (IFOV) of a group of adjacent spatial samples. The slit consists of a 100 μm wide gap etched in a metalized coating on a glass slide and is illuminated by a lamp through a ground-glass diffuser. The entire slit-illuminator assembly is mounted on a computer-controlled translation stage such that the translation is perpendicular to the slit and located in the focal plane of the collimator. The setup, shown in Figure 9a, is aligned with and centered on the AVIRIS entrance aperture. The slit translation rate is measured using a microscope, dial gauges, and a stopwatch and converted to an angular rate using the focal length of the collimator. Figure 9b shows a typical GRF with a FWHM of 1.12 mrad and a sampling interval of 0.85 mrad.

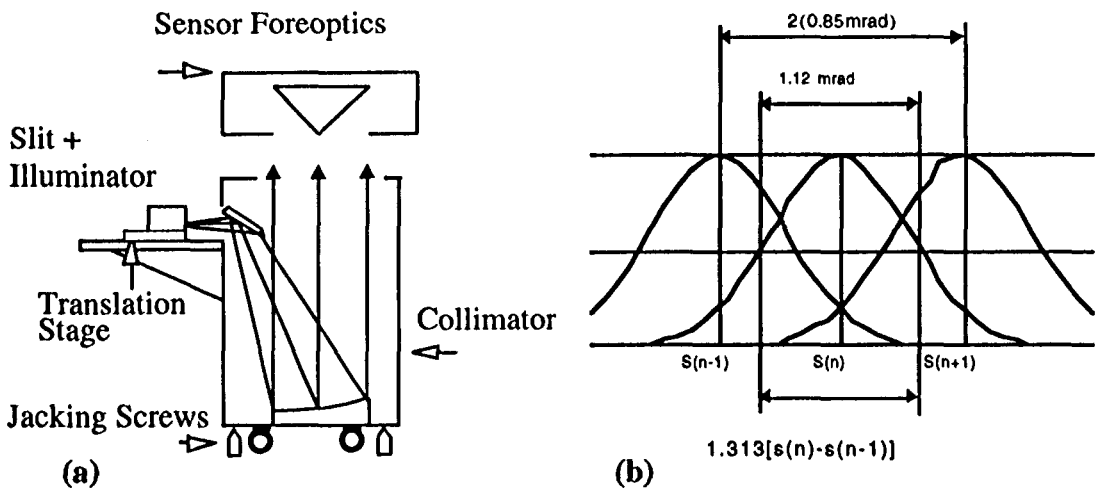

FIGURE 9. (a) Setup for measuring spatial response and sampling, (b) geometric response functions for three adjacent channels.

Data analysis is straightforward. Each along-track line of the response data observes the illuminated slit with a slight shift in angle. The GRF is interpreted as the normalized signal response versus along-track line for a given sample. Lines are calibrated to units of angle equal to slit scan rate [0.4 mrad/s] times AVIRIS scan period [1/12 s]. This moves the slit 1 sample to the right in about 25 along-track scan lines. As the image of the slit moves out of one sample it translates into the adjacent sample. Figure 10 shows the response of sample 270 and sample 271 (2 out of the 614 cross-track samples in the AVIRIS data). This data has been smoothed with a boxcar average to remove line-to-line scan jitter noise related to the GRF measurement technique. The slight asymmetry in the GRF is the result of a detector lag anomaly present in the 1995 and 1996 AVIRIS data. The lag affects both the width and the bore sight of the GRF and appears to be a function of channel brightness and change in channel brightness.

The scan jitter does not affect the shape of the GRF on any line but it does add a random element to line-to-line pointing variation. The smoothed response is shown in Figure 11 along with the raw (unsmoothed) data. A simulated normally distributed line-to-line scan jitter with a standard deviation of 0.07 milliradian closely matches the observed data.

The cross-track field of view of the AVIRIS sensor is determined by the 614 cross-track samples and the 0.85 milliradian sampling and is 30 degrees in extent. Table 1 summarizes the spatial calibration measurements made on 26 April 1996 just prior to the 1995 flight season.

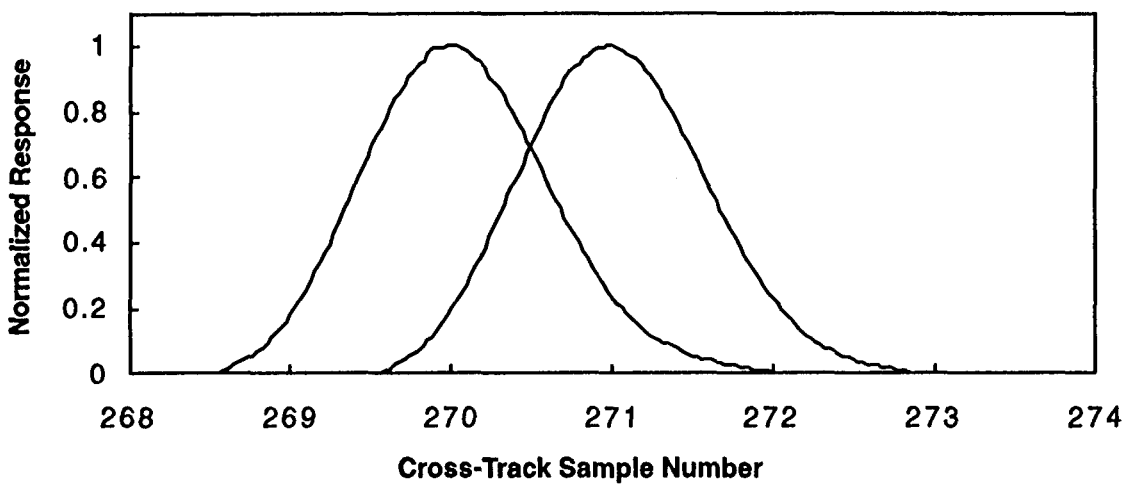

FIGURE 10. Dynamic (scanner-on) cross-track normalized response: Sampling interval is 0.85*FWHM. Asymmetry is the result of residual detector lag present in 1995 AVIRIS data.

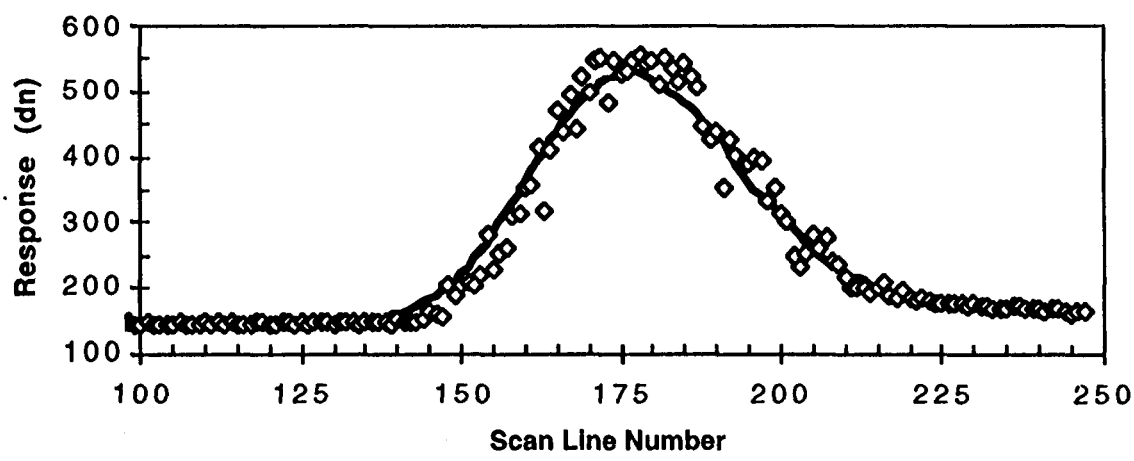

FIGURE 11. Box-car averaged (bold line) and raw (diamonds) dynamic slit response data used to estimate the line-to-line RMS scan jitter.

TABLE 1. Spatial calibration analysis results from 950426 data set. Variation in IFOV and channel alignment between spectrometers is due to a residual detector lag present in the 1995 AVIRIS data.

Spectrometer	A	B	C	D
Dynamic cross-track IFOV	1.12 mrad	1.22 mrad	1.16 mrad	1.25 mrad
Line-to-line RMS jitter	0.07 mrad	0.07 mrad	0.07 mrad	0.07 mrad
Cross-track sampling interval	0.85 mrad	0.85 mrad	0.85 mrad	0.85 mrad
Relative channel alignment to A	-	0.11 mrad	0.09 mrad	0.18 mrad
Static along-track IFOV	1.0 mrad	1.0 mrad	1.0 mrad	1.0 mrad
Static cross-track IFOV	1.0 mrad	1.0 mrad	1.0 mrad	1.0 mrad

5.0 Conclusions

The AVIRIS sensor appears to be meeting the spectral calibration goals of absolute center wavelength knowledge (0.1 nm) and FWHM bandwidth knowledge (0.1 nm) across the spectrum. This accuracy holds in-flight as independently validated using solar and atmospheric absorption features. The onboard calibrator spectral filter data (contained in the pre-cal and post-cal files included with every distributed science data set) may be used to sense wavelength calibration changes (due to inadvertent mechanical shock and residual spectrometer instability) with a 0.1 nm sensitivity.

The laboratory determined radiometric calibration coefficients have been shown to be valid under actual flight conditions when corrected using the signal from the onboard calibrator. An independently determined radiance based upon the MODTRAN3 code and in situ measurements agrees with the laboratory calibrated AVIRIS data to better than the calibration uncertainty. These results may indicate that NIST overestimates the radiometric uncertainty of irradiance standard lamps. Laboratory calibrated AVIRIS data appear to be limited by atmospheric correction errors rather than instrumental signal-to-noise ratio, instrument response instability, or laboratory calibration inaccuracies.

Techniques for measuring the AVIRIS spatial characteristics are presented along with a set of results from a recent spatial calibration. A detector lag anomaly present in the 1995 and 1996 data has an impact on both the GRF width and inter-channel bore sight.

6.0 Acknowledgments

This research was carried out by the Jet Propulsion Laboratory, California Institute of Technology, under contract with the National Aeronautics and Space Administration.

7.0 References

Anderson, G. P., J. Wang, and J. H. Chetwynd, "MODTRAN3: An update and recent validations against airborne high resolution interferometer measurements," Summaries of the Fifth Annual JPL Airborne Earth Science Workshop, JPL Publication 95-1, Vol. 1, Jet Propulsion Laboratory, Pasadena, California, pp. 5-8, 1995.

Chrien, T. G., M. Eastwood, R. O. Green, C. Sarture, H. Johnson, C. Chovit, and P. Hajek, "Airborne Visible/ Infrared Imaging Spectrometer (AVIRIS) onboard calibration system," Summaries of the Fifth Annual JPL Airborne Earth Science Workshop, JPL Publication 95-1, Vol. 1, Jet Propulsion Laboratory, Pasadena, California, pp. 31-32, 1995.

Chrien, T. G., and R. O. Green, "Instantaneous field of view and spatial sampling of the Airborne Visible/ Infrared Imaging Spectrometer (AVIRIS)," Summaries of the Fourth Annual JPL Airborne Geoscience Workshop, JPL Publication 93-26, Vol. 1, Jet Propulsion Laboratory, Pasadena, California, pp. 23-26, 1993.

Chrien, T. G., R. O. Green, M. L. Eastwood, "Accuracy of the spectral and radiometric laboratory calibration of the Airborne Visible/Infrared Imaging Spectrometer (AVIRIS)," SPIE Vol. 1298, Imaging Spectroscopy of the Terrestrial Environment, pp. 37-49, 1990.

Green, R. O., J. E. Conel, J. Margolis, C. Chovit, J. Faust, 1996, "In-flight calibration and validation of the Airborne Visible/Infrared Imaging Spectrometer (AVIRIS)," Summaries of the Sixth Annual JPL Airborne Earth Science Workshop, JPL Publication 96-20, Vol. 1, Jet Propulsion Laboratory, Pasadena, California, 1996 (this volume).

Green, R. O., "An Improved spectral calibration requirement for AVIRIS," Summaries of the Fifth Annual JPL Airborne Earth Science Workshop, JPL Publication 95-1, Vol. 1, Jet Propulsion Laboratory, Pasadena, California, pp. 75-78, 1995a.

Green, R. O., "Determination of the in-flight spectral calibration of AVIRIS using atmospheric absorption features," Summaries of the Fifth Annual JPL Airborne Earth Science Workshop, JPL Publication 95-1, Vol. 1, Jet Propulsion Laboratory, Pasadena, California, pp. 71-74, 1995b.

Green, R. O., J. E. Conel, M. Helmlinger, J. van den Bosch, C. Chovit, and T. Chrien, "Inflight calibration of AVIRIS in 1992 and 1993," Summaries of the Fourth Annual JPL Airborne Geoscience Workshop, JPL Publication 93-26, Vol. 1, Jet Propulsion Laboratory, Pasadena, California, pp. 69-72, 1993.

Green, Robert O., "Use of Data from the AVIRIS Onboard Calibrator," Summaries of the Fourth Annual JPL Airborne Geoscience Workshop, JPL 93-26, Jet Propulsion Laboratory, Pasadena, California, 1993.

Green, Robert O., Steven A. Larson and H. Ian Novack, "Calibration of AVIRIS digitized data", Proceedings of the Third Airborne Visible/Infrared Imaging Spectrometer (AVIRIS) Workshop, JPL Publication 91-28, Jet Propulsion Laboratory, Pasadena, California, 1991.

Vane, G., R. O. Green, T. G. Chrien, H. T. Enmark, E. G. Hansen, and W. M. Porter, "The Airborne Visible/ Infrared Imaging Spectrometer (AVIRIS)," Remote Sens. Environ., 44:127-143 (1993).

Vane, G., T. G. Chrien, E. A. Miller, J. H. Reimer, "Spectral and radiometric calibration of the Airborne Visible/Infrared Imaging Spectrometer," SPIE Vol. 834, Imaging Spectroscopy II, pp. 91-105, 1987.

8.0 Additional Reading

Sarture, C. M., T. G. Chrien, R. O. Green, M. L. Eastwood, J.J. Raney, and M. A. Hernandez, "Airborne Visible/Infrared Imaging Spectrometer (AVIRIS): sensor improvements for 1994 and 1995," Summaries of the Fifth Annual JPL Airborne Earth Science Workshop, JPL Publication 95-1, Vol. 1, Jet Propulsion Laboratory, Pasadena, California, pp. 145-148, 1995.